

Data Analysis for the G^0 Experiment: Characterization of the Beam Halo

A thesis submitted in partial fulfillment of the requirement of the
degree of Bachelor of Science with Honors in Physics
from the College of William and Mary in Virginia,

by

Aimee C.E. Slaughter

Accepted for _____

Advisor: Prof. David Armstrong

Prof. Todd Averett

Prof. Henry Krakauer

Prof. Nahum Zobin

Williamsburg, Virginia
May 2004

Contents

| | |
|---|-----------|
| List of Figures | 3 |
| Abstract | 4 |
| 1 Introduction | 5 |
| 2 Physics Background | 7 |
| 2.1 Theory | 8 |
| 2.2 JLab Overview | 9 |
| 2.3 G^0 Experiment | 10 |
| 2.4 Beam Halo | 11 |
| 3 Methods | 15 |
| 4 Analysis and Interpretation of Results | 18 |
| 5 Conclusions | 31 |
| 6 Acknowledgements | 33 |
| A Sample Code | 35 |

List of Figures

| | | |
|-----|--|----|
| 2.1 | Schematic of the G^0 Spectrometer Showing Target, Superconducting Coils, and Detectors | 11 |
| 2.2 | Positions of the Halo Target and Halo Monitors 3-6 Along the Beampipe (overhead view). The Beam enters from the left and passes through the hole of the halo target. The beam halo will strike the carbon block around the hole and create a shower, which the monitors can then detect. | 13 |
| 2.3 | Positions of Halo Monitors 1 and 2 in the Beam Alcove (overhead view). | 14 |
| 3.1 | Halo 3, signal triggered on discriminated signal. Voltage vs. time. | 16 |
| 3.2 | Halo 4, signal triggered on discriminated signal. Voltage vs. time. | 16 |
| 3.3 | Placement of Detectors Halo3 and Halo4 Along Beam Line | 17 |
| 4.1 | Suspicious Halo Monitor Changes: The rates for four Halo detectors are plotted vs. time. The jump at -10 minutes is a beam trip. | 18 |
| 4.2 | January Ratios of Related Monitors vs. Run Number. | 20 |
| 4.3 | January Ratios of Less Related Monitors vs. Run Number. | 20 |
| 4.4 | March Ratios of Related Monitors vs. Run Number. | 21 |
| 4.5 | March Ratios of Less Related Monitors vs. Run Number. | 21 |

| | | |
|------|---|----|
| 4.6 | January Singles Rates vs. Run Number in North American Detectors. | 22 |
| 4.7 | January Singles Rates vs. Run Number in French Detectors. | 23 |
| 4.8 | March Singles Rates vs. Run Number in North American Detectors. | 24 |
| 4.9 | March Singles Rates vs. Run Number in French Detectors. | 25 |
| 4.10 | Beam Trip in Run 21168. The y-axis is current in units of microamps and the x-axis is time in units of 30 Hz. | 26 |
| 4.11 | First Three Steps in Beam Current After Beam Trip in Run 21168. The y-axis is current in units of microamps and the x-axis is time in units of 30 Hz. | 27 |
| 4.12 | Halo 3 During the First Three Steps in Beam Current After Beam Trip in Run 21168. The y-axis is halo rate in units of Hz and the x-axis is time in units of 30 Hz. | 27 |
| 4.13 | Raw Halo Rates for Beam Current Monitor Calibration Runs 20481 | 28 |
| 4.14 | Normalized Halo Rates for Beam Current Monitor Calibration Runs 20481 | 29 |
| 4.15 | Run 20481, X-Position of the Beam, as measured by the H00CXP monitor, vs. time in units of 30 Hz. Note: the first group of data where the beam was in the wrong position (nominal position is about 48000). | 29 |
| 4.16 | Run 20481, Y-Position of the Beam, as measured by the H00CXP monitor, vs. time in units of 30 Hz. Note: the first group of data where the beam was in the wrong position (nominal position is about 48000). | 30 |

Abstract

All matter is based on protons and neutrons, and these in turn are made up of quarks. The uncertainty principle allows for a “sea” of quark-antiquark pairs inside protons and neutrons, in addition to the three quarks that are their main structure. The focus of the G^0 experiment at Jefferson Lab is the contribution of the strange quark to the character of the proton. The effects of different flavors of quarks can be disentangled by combining theory and experiment; the weak interaction can also be isolated for study because it violates parity symmetry. The electron beam being collided with the proton target in the experiment, however, carries with it a halo. This beam halo is a non-Gaussian fringe caused by interactions with stray gas in the beam enclosure, the beamline, the beam itself, etc. The halo could adversely affect the results of the experiment, especially if it is helicity-correlated, since G^0 is a parity violation experiment. It is therefore important to characterize the beam halo, which is monitored with a halo target (of two possible sizes) and several halo monitors. The halo monitors themselves are characterized to investigate the extent of their reliability and applicability. After establishing this, the halo rates are analyzed in several ways to determine what sort of beam halo the experiment usually has to contend with. Overall, it seems that the halo monitors perform as expected. Having the halo monitors and target in place during experimental runs provides valuable insight into the quality of the beam.

Chapter 1

Introduction

There is a fundamental human curiosity about how things work and what things are made of. We have found that all matter is comprised of atoms, and atoms themselves of protons, neutrons, and electrons (protons and neutrons are collectively referred to as nucleons, since they create the nucleus). Now it is apparent protons and neutrons also have a substructure: a trio of quarks. The proton, for example, has a primary structure of two up quarks and a down quark. Quarks come in six flavors: up, down, strange, charm, top, and bottom. Each flavor has distinctive properties.

Quarks stay bound together in a nucleon by exchanging gluons, the carriers of the strong force. The uncertainty principle allows for the creation of virtual particle-antiparticle pairs during such exchanges, so along with the one down and two up quarks in the proton, there is also a sea of virtual quark-antiquark pairs. The lifetime for a quark-antiquark pair is inversely related to the mass of the quark, so the strange quark, which is the third lightest flavor after up and down quarks, is expected to have the greatest effect in the proton's virtual sea.

The influences of this sea on the properties of the proton or neutron are quite interesting and not yet suitably explained by theory. Experimental guidance is needed, and thus the G^0 experiment[1] at the Thomas Jefferson National Accelerator Facility (JLab) was undertaken. By colliding a beam

of polarized electrons with an unpolarized proton target, G^0 aims to uncover many of the effects of the strange quark on the proton sea. The interactions between the beam and target are governed by both electromagnetic and neutral weak forces. The electromagnetic and weak couplings of each quark are different, and so the effects of each flavor can be disentangled from each other. The weak interaction can be isolated for study because it violates parity symmetry: there is a difference in the scattering rates of electrons with their spins aligned with their momentum and those with oppositely aligned spins. For confidence in the results, however, we must understand the character of the electron beam. The beam may carry a halo – a non-Gaussian tail of extraneous electrons around the beam itself – which would interfere, perhaps significantly, with the data if not corrected for.

Chapter 2

Physics Background

The data from G^0 will illuminate properties of nucleons, and the effects of their quark seas, as yet unknown. Understanding some of the theory about quarks is therefore useful (for a more detailed discussion of this, see [2]). Just as quantum electrodynamics (QED) describes the exchange of photons between charges, quantum chromodynamics (QCD) describes the exchange of gluons between quarks. From the Standard Model we know that photons are the force carrier particle for the electromagnetic force and that gluons carry the strong force; photons, however, carry no charge while gluons carry both a color and an anticolor (that do not result in net colorlessness). QCD is like QED in that opposite colors attract and like colors repel. It can also be shown that anti-symmetrical quantum states cause different colors to attract and symmetrical quantum states cause different colors to repel. Interestingly, QCD does not require the existence free quarks to be forbidden. It actually allows for asymptotically free quarks in the limit of high Q^2 , where Q^2 is the momentum transfer.

Experimentally, it has been found that the effect of antistrange and strange quarks on the longitudinal momentum of protons and neutrons (collectively named nucleons) is of the same order (several percent) of antiup and antidown quarks' effect.[3] The contribution of strange quarks to

nucleon charge and magnetism can be found by combining existing measurements of nucleon electromagnetic form factors and parity-violating electron scattering experiments such as G^0 . Parity violation is essential here, because that is the key to disentangling the effects of the different quark flavors. The photons' coupling to quarks is proportional to the electric charge of the quarks; similarly, the Z^0 's coupling is directly related to the weak charge of the quarks. The interference of electromagnetic and weak currents violates parity because the weak interaction violates parity, thus measurements sensitive to γ and Z^0 exchange allow the different quark flavors to be isolated.

2.1 Theory

Letting $f = \text{flavors}$, the elementary quark currents in the nucleon are:

$$J_\mu^i = \langle N | \sum_f e_f^i \bar{q}_f \Gamma_\mu q_f | N \rangle \quad (2.1)$$

where i encodes electromagnetic or neutral weak currents, and Γ_μ is γ_μ for vector currents and $\gamma_\mu \gamma_5$ for the weak axial current.[4] The axial current G_A and electromagnetic and weak form factors, $G_{E,M}^\gamma$ and $G_{E,M}^Z$, respectively, are of interest to us, and can be defined in the following way[4]:

$$G_A = G_A^u - (G_A^d + G_A^s) \quad (2.2)$$

$$G_{E,M}^\gamma = \frac{2}{3} G_{E,M}^u - \frac{1}{3} (G_{E,M}^d + G_{E,M}^s) \quad (2.3)$$

$$G_{E,M}^Z = (1 - \frac{8}{3} \sin^2 \theta_W) G_{E,M}^u + (-1 + \frac{4}{3} \sin^2 \theta_W) (G_{E,M}^d + G_{E,M}^s) \quad (2.4)$$

Assuming charge symmetry, these equations, which hold true for the proton, can be expressed for the neutron by exchanging u for d , \bar{u} for \bar{d} , and vice versa. Charge symmetry is an important

assumption here[5]: if this symmetry holds, nucleons only differ by the exchange of up and down quarks. G_E and G_M are essentially Fourier transforms of the charge and current distributions.

An experimental asymmetry arises because of the parity violation. Denoting the cross-sections from right- and left-handed electrons by σ_R and σ_L , the asymmetry can be expressed as

$$A = \frac{\sigma_R - \sigma_L}{\sigma_R + \sigma_L}. \quad (2.5)$$

This asymmetry is specifically

$$A = -A_0 \tau (2 - 4 \sin^2 \theta_W - \frac{\varepsilon G_E^0 + \tau G_M^0}{\varepsilon G_E^{\gamma p} + \tau G_M^{\gamma p}}) - A_A \quad (2.6)$$

in the case of elastic scattering off the proton, where (given G_F as the Fermi coupling constant, m_p as the mass of the proton, and α as the fine structure constant):

$$A_0 = \frac{G_F m_p^2}{\sqrt{2} \pi \alpha}, \quad (2.7)$$

θ_W is the Weinberg angle, $\varepsilon = [1 + 2(1 + \tau) \tan^2 \frac{\theta}{2}]^{-1}$, $\tau = 4Q^2/m_p^2$, and

$$G_{E,M}^0(\tau) = \frac{1}{3} (G_{E,M}^u + G_{E,M}^d + G_{E,M}^s). \quad (2.8)$$

A_A is the axial vector form factor, which is small at forward scattering angles; ε and τ are kinematical factors.

2.2 JLab Overview

The experiment suggested by the above theory requires a rather involved setup: namely, a particle accelerator. At JLab there is an electron beam available to three experimental halls simultaneously.

The beam is created at the injector, by polarized laser light incident on strained-layer GaAs wafers in a 100 kV electron gun. The crystal being strained is useful because the $m = \frac{3}{2}$ spin states have been forced out of having the same energy, so the laser can be tuned to a frequency that targets the $\pm\frac{3}{2}$ states that can then promote an electron to either of the two high-energy $m = \frac{1}{2}$ spin states. The GaAs photo-cathodes are exposed to atomic hydrogen to clean the surface and then the activation energy of the surface is reduced by introducing Ce and then nitrogen trifluoride. There are three separate laser systems, one for each hall; and each has an optical pulse train locked to the accelerator's radio frequency. For G^0 , a Ti:Saph laser is required, rather than the regular diode laser, to achieve an electron beam repetition rate of 31.1875 MHz and average current of $40\mu\text{A}$. [6]

The electron beam leaves the injector, and enters the ring. The ring is ovoid and comprised of two linear accelerators connected by two half-turns. The linacs accelerate the electrons in bursts by channelling them through RF cavities. A series of dipole magnets take the beam around the turns, and quadrupole magnets focus the beam. Each quadrupole magnet focuses the beam along one axis. The electrons make up to five passes before being diverted into one of the three experimental halls.

2.3 G^0 Experiment

G^0 is underway in Experimental Hall C. It derives its name from G_E^0 and G_M^0 , the elastic flavor-singlet form factors being measured. G_E^0 is the charge form factor, and G_M^0 the magnetic. G^0 is taking the first direct measurements of the quark-antiquark sea in low energy observables. [7]

Shown in *Figure 2.1* is the toroidal superconducting spectrometer being used in G^0 . It covers a range of angles and momenta. The detectors are arranged in octants around the "Ferris Wheel;" four of the octants are the responsibility of the North American part of the collaboration, and four are of the French. Each octant has 16 pairs of scintillators, each pair defining a layer of the detector [8].

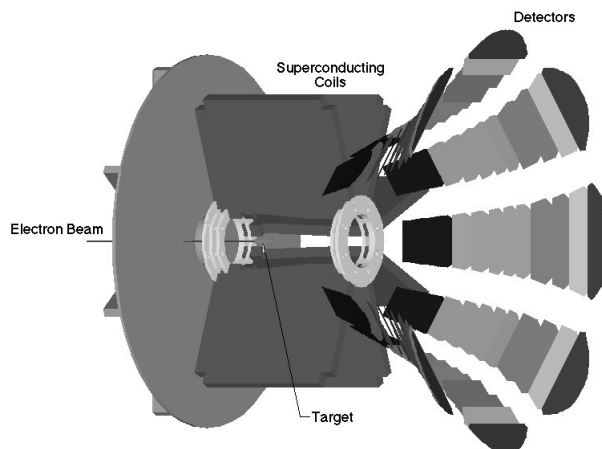


Figure 2.1: Schematic of the G^0 Spectrometer Showing Target, Superconducting Coils, and Detectors

To investigate the parity violation central to the experiment, the electron beam is flipped at 30 Hz between the two helicity states—that is, with the electrons’ momentum aligned and anti-aligned with their spin.

G^0 has a broad Q^2 range, between .12 and 1.0 GeV^2 in the forward orientation and at .25, .5, and .8 GeV^2 in the backward orientation. The electron beam runs at 3.0 GeV and 40 μA , colliding with a 20 cm liquid H target. There are forward and backward orientations of the detecting equipment. The forward set-up measures at small angles where G_E^0 dominates, and detects recoil protons; the backward set-up measures at larger angles where G_M^0 is dominant and detects scattered electrons. Protons will be separated from pions in the forward configuration using time-of-flight measurements; in the backward configuration Cerenkov counters and another scintillator array will be needed.

2.4 Beam Halo

It is not empirically obvious whether the beam halo could be correlated with the helicity of the electron beam. If it were, a false asymmetry would very easily be created. The formation of beam

halo in a high-energy electron accelerator is not well understood, but probable causes include the electron beam scraping the beam pipe, scattering against stray gas in the beam line enclosure, or self-interacting. Halo might also arise from refracted or scattered laser light hitting the photocathode surface in the electron source[9]. Monitoring and characterizing the beam halo ensures that it stays within the experiment's specifications and also allows it to be actively minimized (by adjusting beam steering, etc.).

Halo can interfere in several ways with the data from the experiment: it increases the “singles” rates in the detectors (events not coincident with an event in another detector that are likely due to background) and the general background radiation, lowering the lifetime of the photomultiplier tubes (PMTs) and increasing the dead time (time spent recording background or noise rather than data) in the detectors. The halo could also interact with the target cell walls, which would increase the number of inelastic protons measured; the subtraction of the effect of the inelastic protons under the elastic proton peak is a major contribution to the uncertainty in the G^0 experiment. The halo could also possibly be helicity-correlated, which could then create a false asymmetry, since G^0 is a parity-violation experiment. The requested limit for the halo on the G^0 experiment is 1 part per million (ppm) outside a 6 mm radius. By better understanding the beam halo, verifying whether it's within the specified limit and investigating possible helicity correlation, the uncertainty on the final results of the experiment can be reduced.

To measure the halo both continuously and in specific checks, a sort of “anti-target” is used. The halo targets are holes of specific size in a carbon block through which the beam passes, hopefully centered with the center of the circular hole. The beam (if steered correctly) should pass unaffected through the target hole, while the halo surrounding the beam scrapes against the target sides and creates a shower of particles we can then detect. The two targets are mounted on an apparatus that

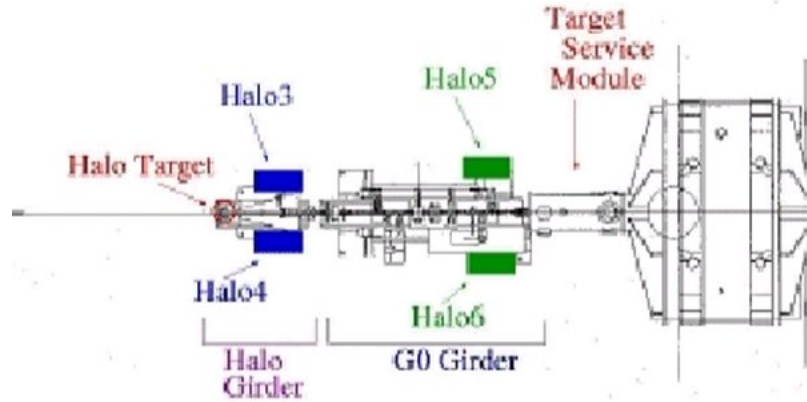


Figure 2.2: Positions of the Halo Target and Halo Monitors 3-6 Along the Beampipe (overhead view). The Beam enters from the left and passes through the hole of the halo target. The beam halo will strike the carbon block around the hole and create a shower, which the monitors can then detect.

allows smooth transitions in and out of the beam, and are of 2 mm-thick carbon, one with a radius of 6 mm for specific checks and one of 11 mm radius for continuous monitoring. The smaller-radius target is used primarily for spot checks since it is right on the edge of the requested halo limit. The 11 mm target gives the beam some leeway for slightly errant steering or halo, but is small enough to be a very useful check on the size of the halo. Either one of the targets or neither of them can be present in the beam, depending on what sort of run is being taken. There is an array of six detectors downstream from (further along the beamline than) the target; the positions of the four downstream detectors considered here, Detectors 3-6, are shown in *Figures 2.2*. *Figure 2.3* shows Halo Monitors 1 and 2, which are upstream of the detector, about where the beam enters Hall C. They provide a useful measure of beam halo coming into the hall before it passes through the halo target.

The halo monitors are photomultiplier tubes (PMTs) attached to scintillators. An incoming particle interacts with the piece of scintillating material in such a way to create a low-energy (bluish-

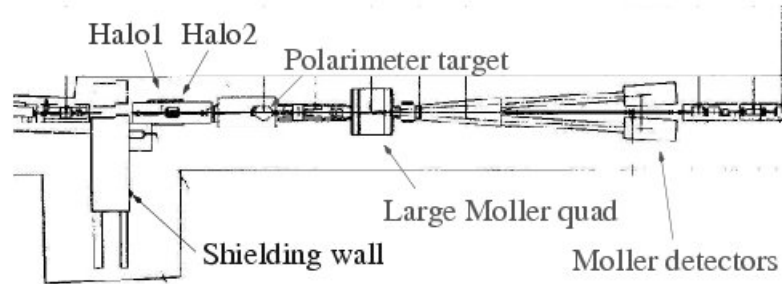


Figure 2.3: Positions of Halo Monitors 1 and 2 in the Beam Alcove (overhead view).

purple or near-UV) photon, which can then strike the PMT face. Traveling through the glass face, the photon hits the photocathode, and an electron is created as described by the photoelectric effect. There are then a series of dynodes which attract and accelerate the photon; at each dynode more electrons are created until the last dynode is reached and there are enough electrons to form an electronic signal which can be processed. Therefore, despite their name, PMTs do not create photons but electrons: what they multiply is the signal from one photon striking the PMT.

Chapter 3

Methods

William and Mary physics graduate student Sarah Phillips and I installed two halo detectors, Halos 3 and 4, in Hall C. Each detector is a PMT coupled via a silicone cookie with a small piece of scintillator; the whole detector is wrapped in Tedlar and black electrical tape to ensure that it is light-tight. We worked to characterize the detectors before we put them in place in the hall. Plots characterizing both detectors are shown in *Figures 3.1* and *3.2* – in these measurements the signals from the detectors have been fed through a discriminator before being sent to the oscilloscope as the trigger, with the undiscriminated signal being displayed. Thus it is an undiscriminated signal being shown in the figures, but the oscilloscope displayed this signal based on the discriminated signal. These signals demonstrate healthy PMTs. The rise time is quick (around 3 nanoseconds). There are more shallow curves than deep ones: the shallowest ones represent single photoelectron events, while the deeper ones probably result from cosmic rays.

The positions of Halo 3 and 4 along the beam line are shown in *Figure 3.3*. We mounted them on aluminum ledges on either side of the halo girder.

Once the halo monitors were installed in the hall and the experiment started to run, the data had to be analyzed. There is a huge volume of information being collected every moment the beam is on,

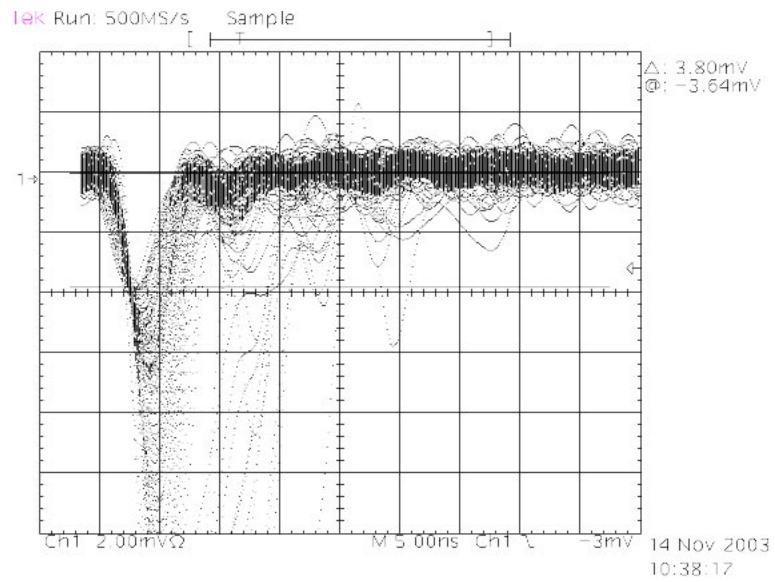


Figure 3.1: Halo 3, signal triggered on discriminated signal. Voltage vs. time.

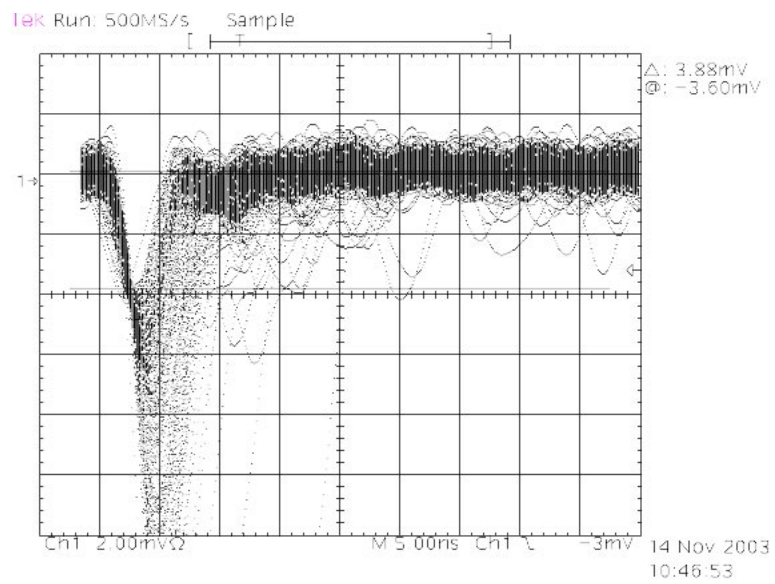
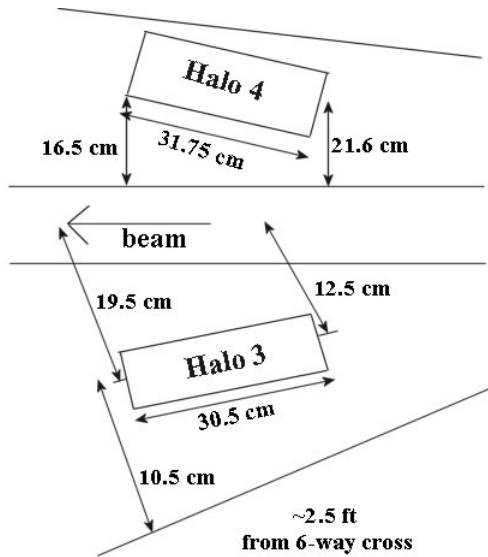


Figure 3.2: Halo 4, signal triggered on discriminated signal. Voltage vs. time.



(image not to scale)

Figure 3.3: Placement of Detectors Halo3 and Halo4 Along Beam Line

so the relevant numbers have to be selected out of storage for processing. To do this, C++ programs including commands in ROOT[10] and MySQL[11] were needed. C++ provided the framework for the program which then was sent running errands in the other languages to fetch data from the database. The database would then politely return the requested information, and the program could then analyze it and graph the results. Reference [12] is an excellent resource for C (of which C++ is an extension), and proved very helpful. A sample of part of a program written to create graphs of halo rate versus beam current is provided in the appendix.

Chapter 4

Analysis and Interpretation of Results

While the experiment is running, the halo monitors give a window into the beam quality. If the halo rates were to suddenly increase, as shown in *Figure 4.1*, the run leader would be wise to stop the run and try to correct whatever is causing the large halo.

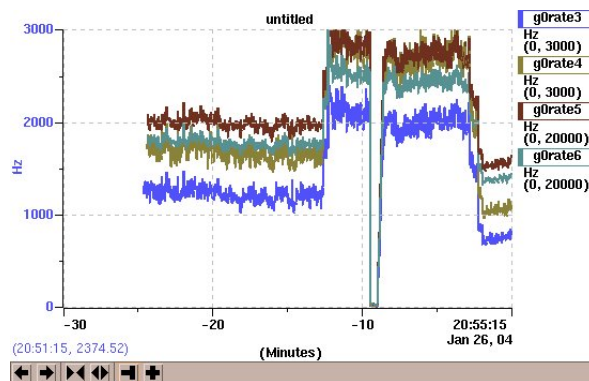


Figure 4.1: Suspicious Halo Monitor Changes: The rates for four Halo detectors are plotted vs. time. The jump at -10 minutes is a beam trip.

In the case of *Figure 4.1*, the halo rates actually increased because of changes made to part of the experimental set-up, which were then changed back to their original settings, bringing the rates back

down to reasonable levels. However, the sort of change shown could be typical of, though probably much larger in size than, an increase in rates that would arise from mis-steering of the beam.

Looking at the average halo rate over many runs can be useful as well. In particular, the ratios between different halo monitors can illuminate how well they respond to different beam situations. The tables below list the status of the halo target during runs through January and March; *Figures 4.2- 4.5* are plots of average halo rate ratios for these runs. Halo monitors 3 and 4, and 5 and 6, are more closely related pairs since each pair has similar high voltage settings and are in mirror positions along the beamline.

| January Runs | | March Runs | |
|---------------------|----------------|---------------------|------------------------------|
| Runs 18992 - 19049: | 11mm target in | Runs 20452 - 20456: | 6mm target in |
| Runs 19050 - 19111: | no halo target | Run 20457: | no halo target, coil pulsing |
| Runs 19112 - 19161: | 11mm target in | Runs 20458 - 20462: | 6mm target in |
| Runs 19162 - 19176: | no halo target | Run 20463: | no halo target, coil pulsing |
| Runs 19177 - 19263: | 11mm target in | Runs 20464 - 20490: | 6mm target in |
| Runs 19264 - 19267: | 6mm target in | Runs 20492 - 20503: | 6mm target in |
| Runs 19268 - 19286: | 11mm target in | Run 20504: | 6mm target, no beam |
| Runs 19287 - 19299: | 6mm target in | Runs 20505 - 20512: | 6mm target in |
| Runs 19300 - 19340: | 11mm target in | Runs 20513 - 20514: | 6mm target in |
| Runs 19340 - 19342: | no halo target | Runs 20516 - 20535: | 6mm target in |
| Runs 19343 - 19417: | 11mm target in | Runs 20537 - 20562: | 6mm target in |
| Runs 19418 - 19571: | 6mm target in | Run 20618: | 6mm target in |
| | | Runs 20619 - 20525: | 11mm target in |
| | | Run 20626: | 6mm target in |
| | | Run 20627: | 6mm target in, coil pulsing |
| | | Run 20628: | no halo target, coil pulsing |
| | | Runs 20629 - 20634: | 6mm target in |
| | | Runs 20656 - 20658: | 6mm target in |
| | | Runs 20672 - 20677: | 6mm target in |
| | | Runs 20678 - 20679: | 6mm target in, no beam |
| | | Runs 20680 - 20778: | 6mm target in |

It is perhaps more interesting to focus on the related monitors, since the ratio between the two appears to be more sensitive to beam conditions. Comparing *Figures 4.2- 4.5* with *Figures 4.6- 4.9* can be elucidating. *Figures 4.6-4.9* show the singles rates over the same runs for one detector (Detector 6) in each octant. Singles are events that are not coincident with any other—that is, events

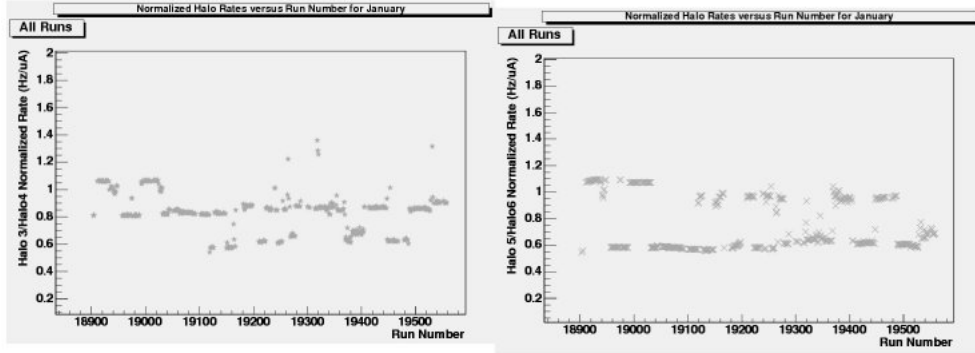


Figure 4.2: January Ratios of Related Monitors vs. Run Number.

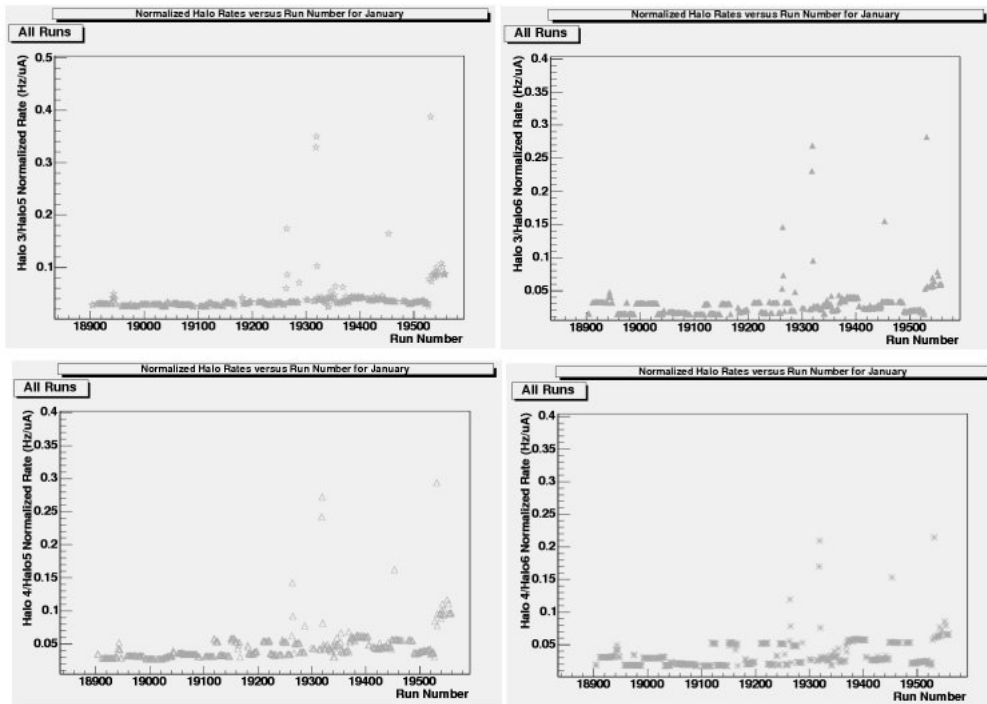


Figure 4.3: January Ratios of Less Related Monitors vs. Run Number.

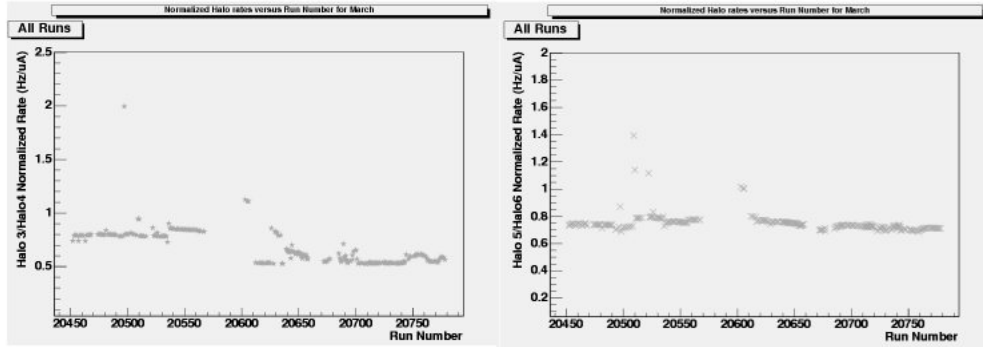


Figure 4.4: March Ratios of Related Monitors vs. Run Number.

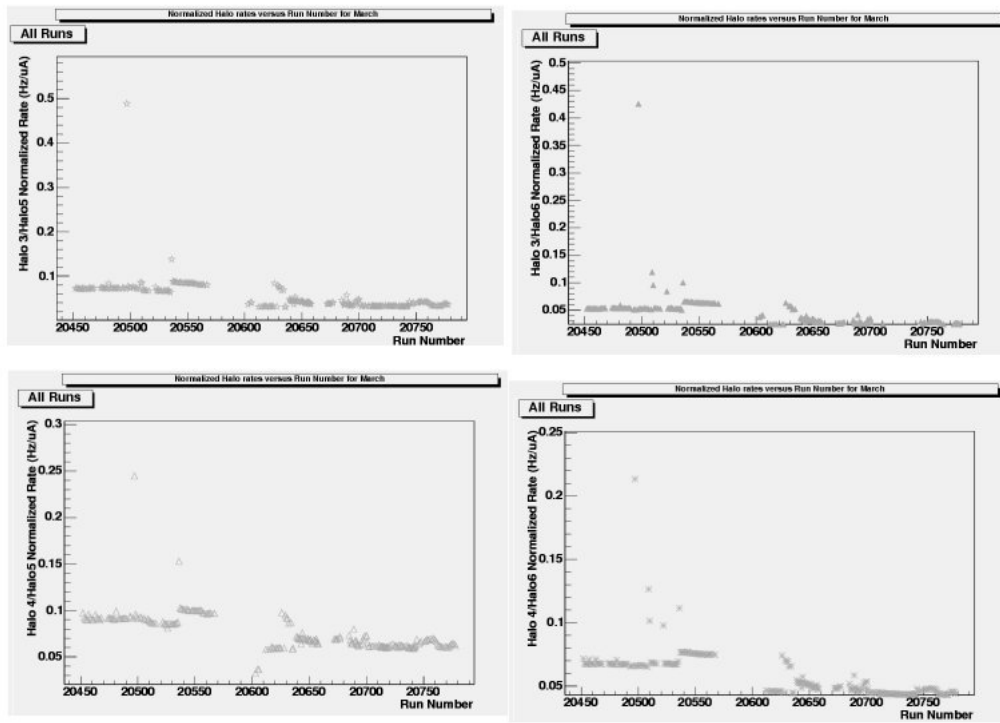


Figure 4.5: March Ratios of Less Related Monitors vs. Run Number.

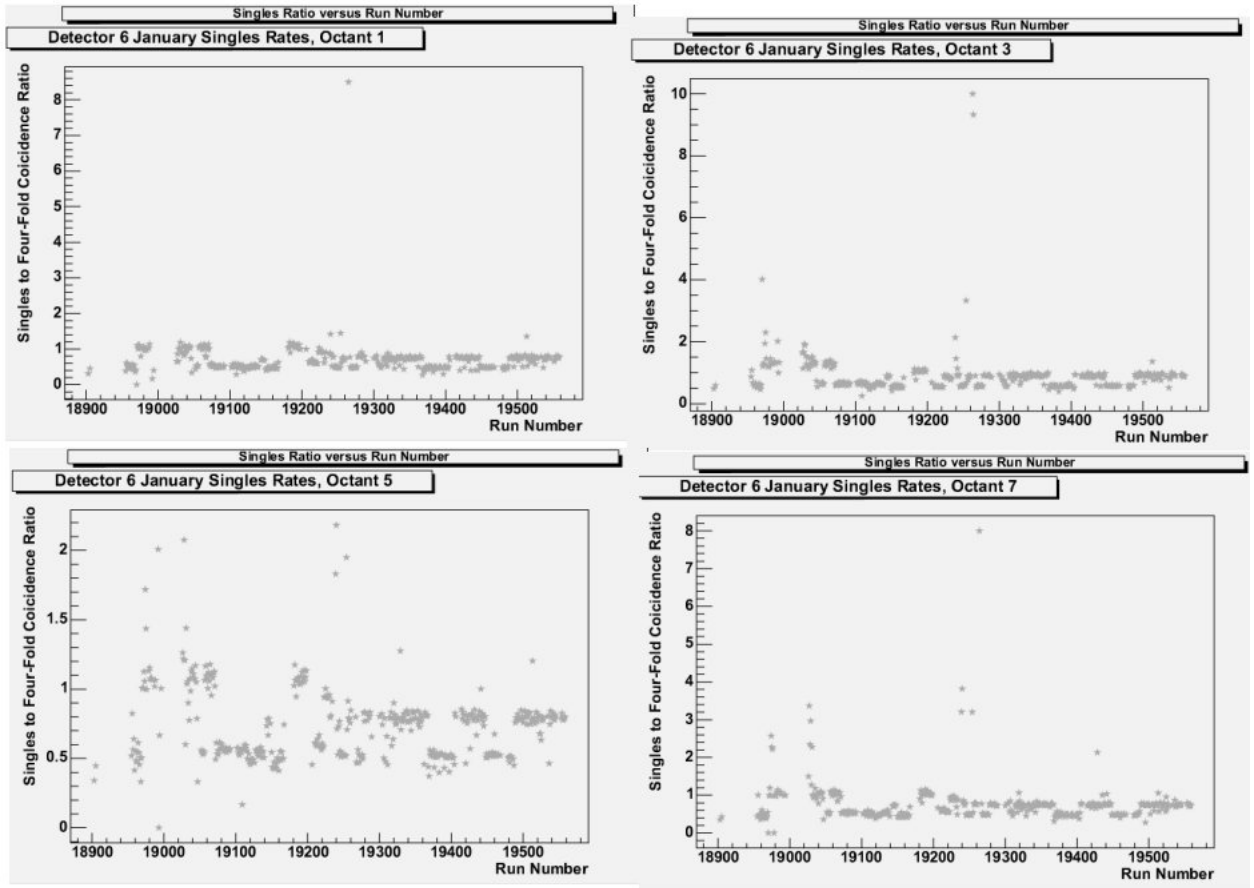


Figure 4.6: January Singles Rates vs. Run Number in North American Detectors.

likely to be related to the background and not to data. The plots group the North American octants (odd numbered) and the French octants (even numbered). From all these plots times of "good beam" and "bad beam" can be observed. From all of the halo ratios, however, it is apparent that the monitors scale together quite well and react in predicted ways to changes of the halo target.

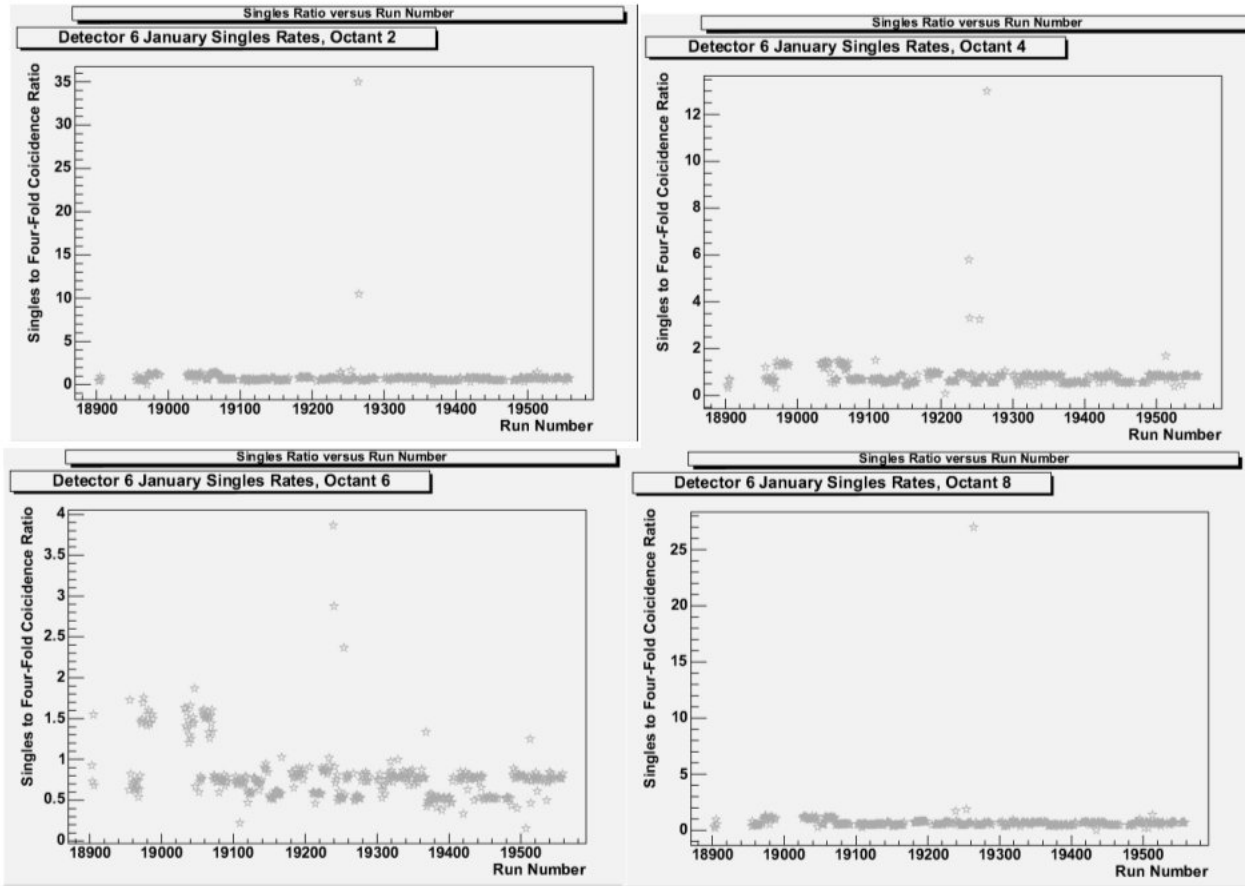


Figure 4.7: January Singles Rates vs. Run Number in French Detectors.

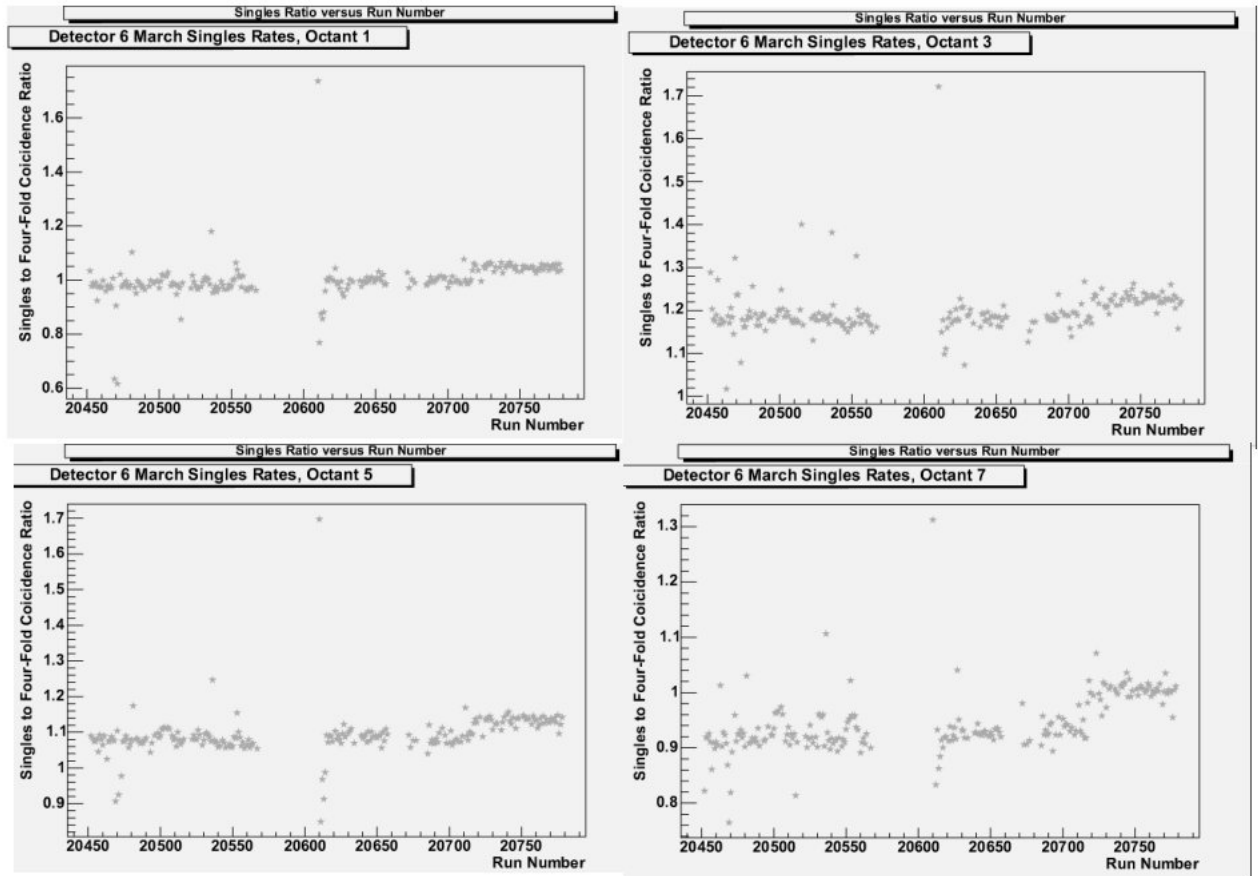


Figure 4.8: March Singles Rates vs. Run Number in North American Detectors.

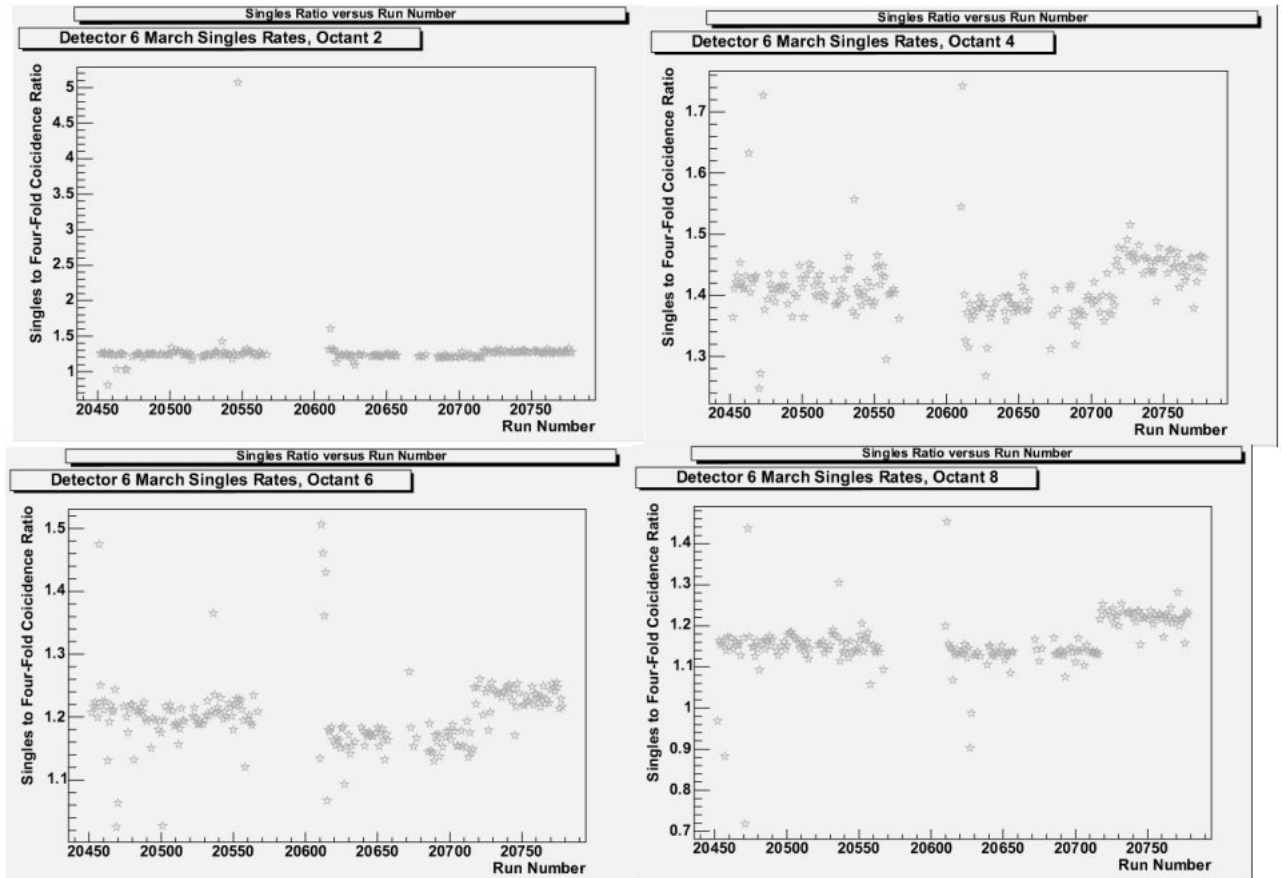


Figure 4.9: March Singles Rates vs. Run Number in French Detectors.

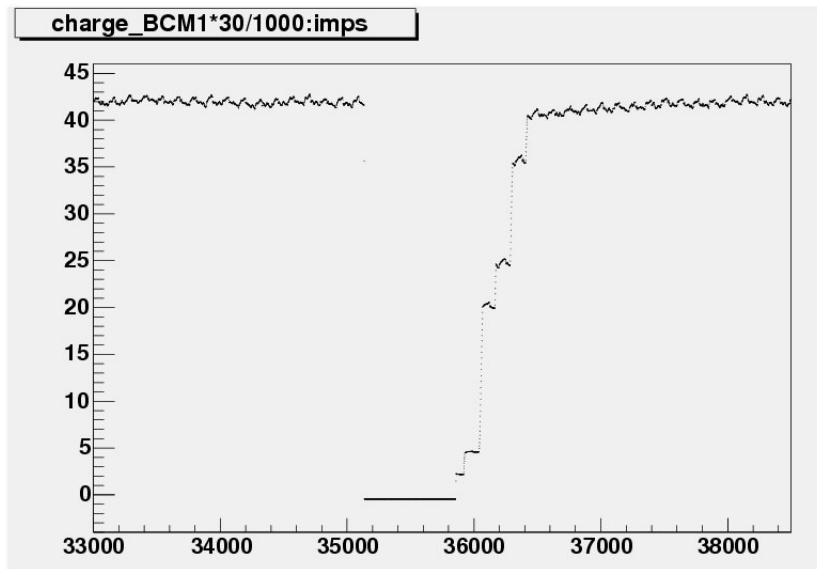


Figure 4.10: Beam Trip in Run 21168. The y-axis is current in units of microamps and the x-axis is time in units of 30 Hz.

To relate the rates from the halo monitors to the beam current (measured by two beam current monitors, BCM1 and BCM2), it's useful to look at times where the beam current is changing in an understood manner. One such time is when the beam is coming back after a beam trip. When the beam trips off, the beam is brought back in small steps until it reaches $40 \mu\text{A}$, as visible in *Figure 4.10*, from Run 21168. BCM1 is multiplied by 30 to account for the 30 Hz cycling between right- and left-handed helicity electrons, and divided by 1000 to change the units from amps to milliamps; imps is a measure of time. *Figure 4.11* shows a closer view of the first three steps of beam coming back. *Figure 4.12* is the same graph, only plotting Halo 3 rather than BCM1. It's evident that there is not enough data in *Figure 4.12* to be statistically significant, or even sensible, so looking into beam trips is not a worthwhile source of halo data.

Since the steps during the ramping up of the beam after a beam trip are too small to yield any

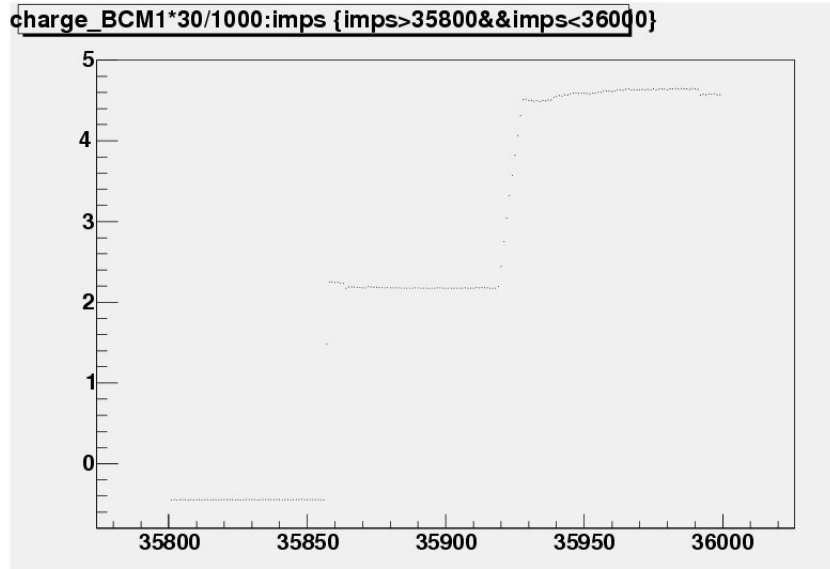


Figure 4.11: First Three Steps in Beam Current After Beam Trip in Run 21168. The y-axis is current in units of microamps and the x-axis is time in units of 30 Hz.

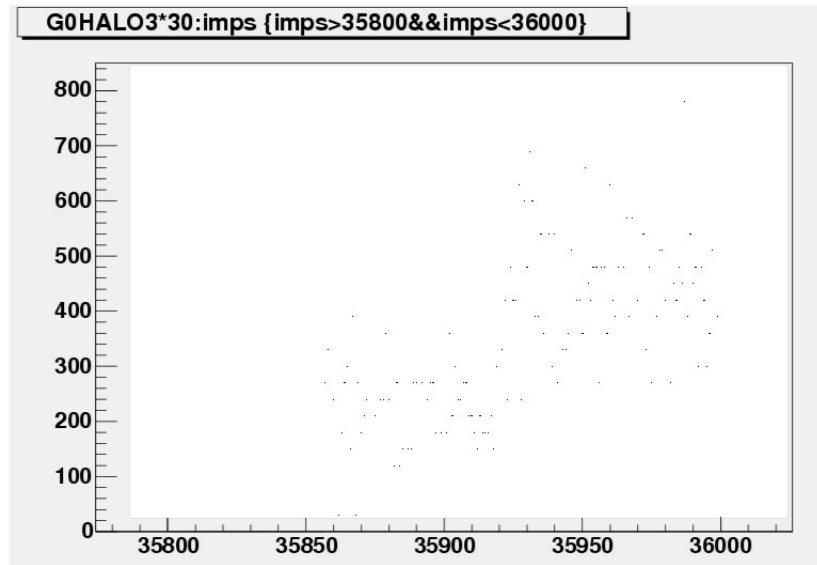


Figure 4.12: Halo 3 During the First Three Steps in Beam Current After Beam Trip in Run 21168. The y-axis is halo rate in units of Hz and the x-axis is time in units of 30 Hz.

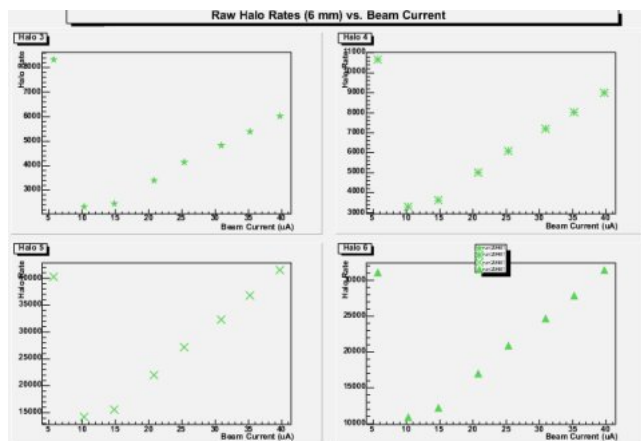


Figure 4.13: Raw Halo Rates for Beam Current Monitor Calibration Runs 20481

useful information, we look instead to BCM calibration runs. In these, the current is stepped up from $5 \mu\text{A}$ to $40 \mu\text{A}$ in $5 \mu\text{A}$ increments. Data from Halos 3-6 from Run 20481, a BCM calibration run with the 6mm halo target in place, was extracted manually from ROOT and then explicitly filled into arrays in a C++ program that then had ROOT plot the results. The raw rates are shown in *Figure 4.13*. The raw rates were then normalized against Run 20352, when the halo target was out of the beam: these normalized rates are shown in *Figure 4.14*. The normalization was achieved by taking the raw rates with the halo target and dividing them by the beam current, and then subtracting from this the raw rates without the halo target divided by the beam current.

From these plots, it is evident that the halo monitors scale together. The run appears fairly linear, so there was no increase in halo during the run. The first point seems abnormally high; this is most likely attributable to beam steering. It is fairly clear, as shown in *Figures 4.15* and *4.16*, that the beam position, in both the x- and y-directions, was off by about a factor of two. It was most likely this measurable difference that caused an increased halo rate, because the mis-steered beam would scrape against the halo target walls and create a shower.

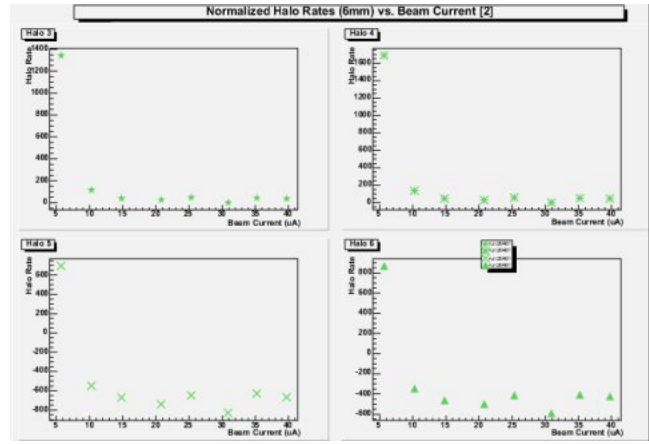


Figure 4.14: Normalized Halo Rates for Beam Current Monitor Calibration Runs 20481

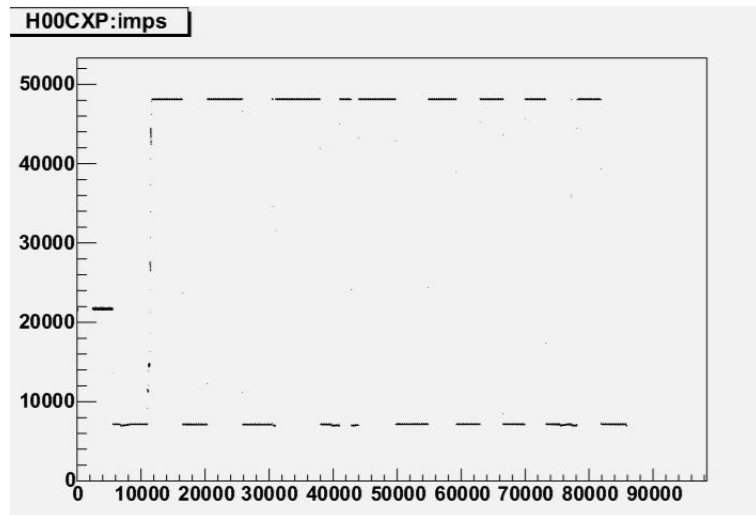


Figure 4.15: Run 20481, X-Position of the Beam, as measured by the H00CXP monitor, vs. time in units of 30 Hz. Note: the first group of data where the beam was in the wrong position (nominal position is about 48000).

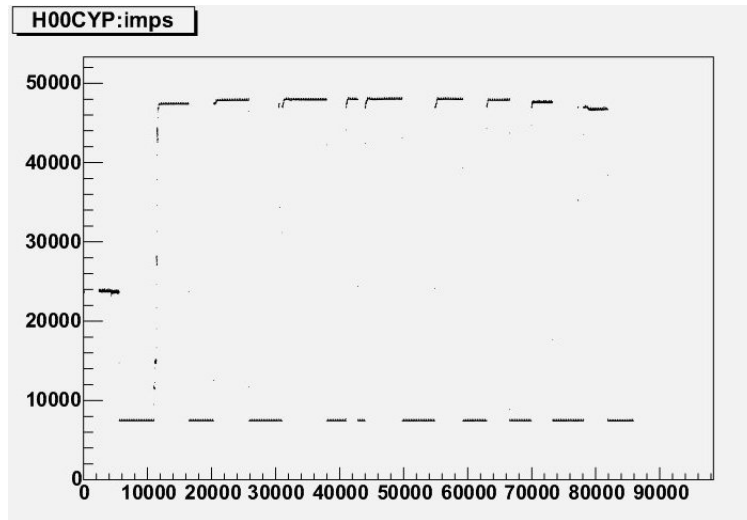


Figure 4.16: Run 20481, Y-Position of the Beam, as measured by the H00CXP monitor, vs. time in units of 30 Hz. Note: the first group of data where the beam was in the wrong position (nominal position is about 48000).

Chapter 5

Conclusions

The raw data this analysis is based on was expected to be in hand beginning in October of 2003. Hurricane Isabel, however, robbed the area of its electricity for several days, which forced JLab's cryo system to be down for the first time. This introduced over a month's worth of work at the lab bringing everything back online, and the G^0 experiment started much later than originally planned. Thus I was unable to start analysis until the spring semester began. Despite this considerable setback, some valuable information has been gleaned. The halo monitors are a very valuable aspect of the beam monitoring system in place while data is being taken on the experiment.

During the fall semester, I worked with Sarah Phillips to characterize and install halo monitors 3 and 4. Halos 3 and 4 performed like healthy PMTs in the lab, responding at appropriate voltage settings with signals with short rise times. We mounted them in the Hall C on either side of the beamline, making them a part of the halo monitor array positioned for continuous monitoring of the electron beam.

Once the experiment began production runs, these halo monitors characterized the beam in real-time, which allowed the run leader to stop a run and correct beam steering if the halo rates were outside the acceptable range (beam steering is often the source of an abnormally high halo rate,

as the beam scraping the sides of the halo target creates a particle shower). Data from the halo monitors also provides a way to analyze the size of the beam halo after the run has been taken, so that an idea of the overall quality of the electron beam can be formed. As explained earlier, the different monitors scale together well, and the relationship between halo rates and beam current is well-established.

Also while the experiment was underway, I took several shifts on the data-taking. Being in the Hall C Counting House (where the experiment is monitored) not only allowed me to directly help with running of the experiment; it also afforded me a better understanding of how the experiment works and where the data is coming from. It is hard to get a feel for the amount of information being collected and the number of people working on the experiment until one goes and participates in the data collection and monitoring.

Setbacks due both to the delayed running of the experiment and to coding difficulties prevented more analysis from being completed. Useful information is yet to be discovered from better comparison of the halo rates to singles rates. Further study of possible correlations between halo rates and backgrounds in the time-of-flight spectra would be extremely worthwhile, since these backgrounds have peaks corresponding to the pions and inelastic and elastic protons created from the beam striking the target. Any relationship between the halo and this background would show an important aspect of how the halo affects the data from the experiment.

Chapter 6

Acknowledgements

The author would very much like to thank Dr. David Armstrong for serving as advisor for this thesis, and for his help and encouragement throughout the year. A large debt of thanks is also due to Sarah Phillips for help especially with coding, but also just about everything else. Everyone at JLab was very welcoming and patient with a new and unexperienced member; Julie Roche and Gary Rutledge were especially helpful. Of course, thanks are also due to the William and Mary physics department (both faculty and students), and last but not least to the members of the honors committee for taking time to evaluate this thesis.

Bibliography

- [1] G0 Home Page. <http://www.npl.uiuc.edu/exp/G0>
- [2] I.S. Hughes, *Elementary Particles*, Cambridge University Press, Cambridge, (1991).
- [3] D.S. Armstrong, *Strange Quark Content of the Nucleon*, Proc. 18th Winter Workshop on Nuclear Dynamics, (2002).
- [4] D.H. Beck and B.R. Holstein, *Nucleon Structure and Parity-Violating Electron Scattering*, International Journal of Modern Physics E, World Scientific Publishing Company, (2001).
- [5] E.J. Beise, *Parity Violation with Electrons and Hadrons*, arXiv:nucl-ex/309008, (2003) [Invited talk at the 17th International IUPAP Conference on Few-Body Problems in Physics].
- [6] P. Adderly, M. Baylac, J. Clark, T. Day, J. Grames, J. Hansknecht, M. Poelker, M. Stutzman, *Jefferson Lab Polarized Source*, Mainz Parity Workshop Proceedings (2002).
- [7] D. Beck, “ G^0 ”: *Measurement of the Flavor Singlet Form Factors of the Proton* [JLab experiment E91017 abstract].
- [8] G0 at IPNO-RDD. <http://ipnweb.in2p3.fr/rdd/G0/>
- [9] Sarah K. Phillips, *Beam Halo in the First G^0 Engineering Run*, Williamsburg, VA (2003) (unpublished) [draft].
- [10] The ROOT System Home Page. <http://root.cern.ch>
- [11] MySQL: The World’s Most Popular Open Source Database. <http://www.mysql.com>
- [12] Brian W. Kerningham and Dennis M. Ritchie, *The C Programming Language*, Prentice-Hall Inc, New Jersey (1978).

Appendix A

Sample Code

Below are sections of a program that creates plots from points extracted manually from the database. Comments are prefaced by //.

```
Int_t graph1(Int_t NumOfFiles,Float_t Beam_Current[],Float_t Beam_Currentb[],Float_t x1[],Float_t
x1b[],Float_t x2[],Float_t x2b[],Float_t x3[],Float_t x3b[],Float_t x4[],Float_t x4b[],char *t);
int main(int argc, char** argv)
{
TApplication theApp("App", &argc, argv);
gStyle->SetOptFit(0111);
//ROOT commands
char t[50];
Int_t NumOfFiles=8;
Float_t x1[NumOfFiles];
//etc. through x4
Float_t x1b[NumOfFiles];
//etc. through x4b
//string, number, and arrays to be filled with data passed to graph1 for each graph created
Float_t Beam_Current[]={5.688,10.27,14.81,20.78,25.32,30.89,35.21,39.72};
//values 20 and above are BCM1, below 20 are BCM2
Float_t Halo3raw[]={8324,2331,2447,3399,4137,4826,5389,6015};
Float_t Halo4raw[]={10660,3305,3625,5010,6090,7194,8030,9002};
Float_t Halo5raw[]={40250,14190,15530,21970,27140,32300,36780,41500};
Float_t Halo6raw[]={31110,10940,12230,17020,20900,24680,27870,31420};
Float_t Beam_Currentb[]={4.969,10.38,15.1,31.04,44.91};
Float_t Halo3rawb[]={1197,2521,3683,2521,3661};
Float_t Halo4rawb[]={1741,3652,5342,3651,5311};
Float_t Halo5rawb[]={6077,13060,19200,13050,19080};
Float_t Halo6rawb[]={4291,9109,13420,9109,13340};
Float_t Beam_Currentnohalo[]={5.187,10.16,14.94,20.32,25.06,29.77,36.09,39.62};
Float_t Halo3nohalo[]={631.8,1115,1869,2750,2893,4572,3926,4452};
Float_t Halo4nohalo[]={968.8,1869,2960,4300,4625,6883,6351,7141};
Float_t Halo5nohalo[]={3994,7885,12480,18360,20340,29370,28210,32460};
Float_t Halo6nohalo[]={3086,5815,9372,13480,14440,22150,20180,22780};
Float_t Halo3[NumOfFiles];
```

```

//etc. through Halo6b
Float_t Halo3n[NumOfFiles];
//etc. through Halo6bn
for (int a=0; a<NumOfFiles; a++) {
Halo3n[a]=((Halo3raw[a]/Beam.Current[a])-(Halo3nohalo[a]/Beam.Currentnohalo[a]));
//etc. through Halo6n
}
for (int b=0; b<NumOfFiles; b++) {
Halo3bn[b]=((Halo3rawb[b]/Beam.Currentb[b])-(Halo3nohalo[b]/Beam.Currentnohalo[b]));
//etc. through Halo6bn
}
//the above for loops create arrays of the normalized halo rate
for(int i=0;i<NumOfFiles;i++) {
x1[i]=Halo3n[i];
//etc through x4b[i]=Halo6bn[i];
}
char title3[50] = "Normalized Halo Rates (6mm) vs. Beam Current [2]\0";
t = title3;
TCanvas* MyCanvas3 = new TCanvas("MyCanvas3", "graph", 1);
graph1(NumOfFiles,Beam.Current,Beam.Currentb,x1,x1b,x2,x2b,x3,x3b,x4,x4b,t);
TString filename3;
filename3 = "/work/hallc/gzero/acslau/g0scratch/scripts/March16/normrates32.jpg";
MyCanvas3->SaveAs(filename3);
theApp.Run();
return(0);
}

Int_t graph1(Int_t NumOfFiles,Float_t Beam_Current[],Float_t Beam_Currentb[],Float_t x1[],Float_t
x1b[],Float_t x2[],Float_t x2b[],Float_t x3[],Float_t x3b[],Float_t x4[],Float_t x4b[],char *t)
{
//this function tells ROOT how to format the graph being created
TPaveLabel* title = new TPaveLabel(0.1,0.96,0.9,0.99,t);
title->Draw();
TDateTime* now;
now = new TDateTime();
TPaveLabel* date = new TPaveLabel(0.7,0.01,0.9,0.03,now->AsString());
date->Draw();
TPad* graphPad1 = new TPad("Graphs", "Graphs",0.01,0.05,0.95,0.95);
graphPad1->Draw();
graphPad1->cd();
graphPad1->Divide(2,2);
graphPad1->cd(1);
TGraph* gr1 = new TGraph(NumOfFiles,Beam_Current,x1);
TGraph* gr2 = new TGraph(NumOfFiles,Beam_Current,x2);
//etc. through gr4b
gr1->SetMarkerColor(8);
gr1->SetMarkerStyle(29);
//etc through gr4b
TMultiGraph* mg1 = new TMultiGraph();

```

```

mg1->SetTitle("Halo 3");
mg1->Add(gr1);
mg1->Draw("AP");
mg1->Add(gr1b);
mg1->Draw("P");
mg1->GetXaxis()->SetTitle("Beam Current (uA)");
mg1->GetYaxis()->SetTitle("Halo Rate");
mg1->Draw("AP");
//TMultiGraph* mg2, mg3, mg4 similarly constructed, substituting for Halo number and gr number
TLegend *leg1;
leg1 = new TLegend(0.45,0.85,0.55,0.99);
leg1->AddEntry(gr1,"run 20481", "p");
leg1->AddEntry(gr2,"run 20481", "p");
leg1->AddEntry(gr3,"run 20481", "p");
leg1->AddEntry(gr4,"run 20481", "p");
leg1->AddEntry(gr1b, "run 20009", "p");
leg1->AddEntry(gr2b, "run 20009", "p");
leg1->AddEntry(gr3b, "run 20009", "p");
leg1->AddEntry(gr4b, "run 20009", "p");
leg1->Draw();
}

```